Acoustic longitudinal mode coupling in w-shaped Al/Ge Co-doped fibre*

Li Hong-Liang(李宏亮)†, Zhang Wei(张 巍),
Huang Yi-Dong(黄翊东), and Peng Jiang-De(彭江得)

State Key Laboratory on Integrated Opto-electronics, Electronic Engineering Department, Tsinghua University, Beijing 100084, *China*

(Received 25 January 2011; revised manuscript received 5 May 2011)

This paper proposes a novel fibre structure aiming at distributed temperature and strain sensing. Utilizing Al_2O_3 and GeO_2 as dopants to form a w-shaped acoustic waveguide, it realizes modal coupling between longitudinal acoustic modes of its inner and outer core layers, leading to a dual-peak or multi-peak Brillouin gain spectrum. The relationship between the acoustic mode coupling properties and the fibre materials, doping concentrations and structural parameters are investigated, showing that the positions of mode coupling points in acoustic dispersion curves and the coupling intensities can be designed flexibly. A specific fibre design for the discriminative sensing of temperature and strain under a pump wavelength of 1.55 μm is given. The responses of its Brillouin gain properties on temperature and strain are analysed theoretically, demonstrating its potential for distributed fibre Brillouin sensing.

Keywords: Brillouin scattering, acoustic mode coupling, fibre sensing, optical fibre design

PACS: 42.82.–i, 42.65.Es, 46.40.–f, 42.81.Pa **DOI:** 10.1088/1674-1056/20/10/104211

1. Introduction

Stimulated Brillouin scattering (SBS) is a nonlinear effect in optical fibre that occurs when the power of incident pump light reaches the Brillouin threshold.[1] The SBS due to the electrostriction effect will generate a modulated refractive index grating in the fibre and arouse back-scattering frequency-downshift stokes waves propagating along the opposite direction against the incident light. The frequency deviations of these counter-propagating Stokes waves, which are also called Brillouin frequency shifts (BFS), are determined by the frequencies of longitudinal acoustic modes in the optical fibre. Since SBS was observed for the first time in 1964, it has been studied intensely in applications such as SBS fibre lasers,[2,3] optical-fibre characterization,[4] slow light systems,[5] and so on.

As BFS is remarkably sensitive to the change of temperature and strain of the fibre, the distributed fibre Brillouin sensor based on SBS has been investigated for more than ten years.[6−10] In order to measure the temperature and strain variation simultaneously, the multi-peak Brillouin gain spectrum (BGS) is needed. The BGS of conventional single mode fibre (SMF) usually has a single-main-peak structure, corresponding to the fundamental acoustic L_{01} mode. In fact, there are some higher-order acoustic modes supported in the acoustic waveguide of the optical fibre, namely, the L_{0i} ($i = 2, 3, \ldots$) modes, however, they make little contribution to the BGS. It is difficult to use optical fibres with this kind of BGS to realize distinguishable temperature and strain sensing. In recent years, some new optical fibre designs focused on realizing the multi-peak BGS are reported, with different dopants in the core and cladding.[11,12] The Brillouin gain peaks in these fibres correspond to several longitudinal acoustic modes and their intensities are always close to each other. Polarization maintaining fibre (PMF) also has the potential to be applied in distributed Brillouin sensing because of its discrimination and independent responses on temperature and strain of BFS, and birefringence along the two orthogonal polarizing axes.[13]

Another approach to generate dual-peak or multi-peak BGS is by making use of microstructure fibre (MSF). Dainese *et al.* investigated multi-peak structure of BGS in MSFs with small cores and some primary analysis on the influence of the cladding

*Project supported in part by the National Natural Science Foundation of China (Grant No. 60777032), 973 Program of China (Grant No. 2010CB327600), and the Science Foundation of Beijing (Grant No. 4102028).

†Corresponding author. E-mail: lhl08@mails.tsinghua.edu.cn

© 2011 Chinese Physical Society and IOP Publishing Ltd

microstructure to the acoustic modes properties are given.[14] In order to illustrate the mechanism of multi-peak BGS in MSF, we have measured the BGS and investigated the influences of the pump wavelength and temperature on BGS of a piece of small-core MSF experimentally.[15] The experimental results can be well explained by the coupling between longitudinal-radial acoustic modes in the MSF. It indicates that the acoustic mode coupling in the fibre will induce a dual or multi-peak BGS structure and its properties are dependent on the enviromental variables, which can be used in multi-parameter fibre sensing. However, the dual-peak BGS properties of MSF are not suitable for the application of Brilouin sensing, because of the low compatibility of MSF to the conventional SMF and its high cost.

Here we propose a novel w-shaped Al/Ge-co-doped optical fibre structure which is able to realize multi-peak BGS through the acoustic longitudinal mode coupling mechanism. The theoretical analysis shows that the mode coupling properties can be adjusted by modulating the optical fibre's structural parameters and doping concentrations in its core and cladding, and the gain peaks of BGS have different responses to the change of temperature and strain, which means that we may conveniently make use of the present optical fibre fabricating method to obtain this kind of fibre that satisfies specific sensing demands.

This paper is organized as follows. The fibre structure and design principle are introduced in Section 2, followed by the theoretical analysis method of acoustic mode and Brillouin gain properties in Section 3. Section 4 provides the illustration of longitudinal acoustic mode coupling in the proposed fibre structure and the adjustment mechanism of mode coupling properties. In Section 5, a specific fibre design, which has a multi-peak BGS at 1.55 μm, is proposed and the influences of temperature and strain on the properties of BGS are studied, showing its potential in fibre sensing. The conclusion is presented in Section 6.

2. Fibre structure

The proposed Al/Ge-co-doped fibre has different waveguide structures for optical and acoustic waves, which are clearly illustrated in the schematic diagram of Fig. 1. The whole optical fibre is divided into four layers: the inner core ($0 < r < a_1$), the inner cladding ($a_1 < r < a_2$), the outer core ($a_2 < r < a_3$) and the outer cladding ($a_3 < r < b$), where r is the radial coordinate in the cylindrical optical fibre, a_1, a_2 and a_3 are radii of the inner-core, inner-cladding and outer-core layers, respectively, and these three parts constitute the core-region, b is the outer-cladding radius (i.e., ∼62.5 μm) and the outer-cladding forms the pure silica cladding-region.

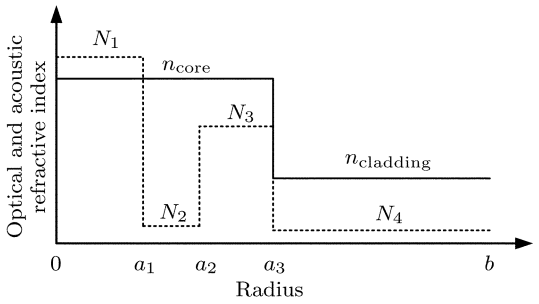


Fig. 1. The optical refractive index n (solid line) and acoustic refractive index N_i (dotted line).

For optical wave transmission, the fibre has a waveguide structure similar to SMF and shows a simple step-like optical refractive index profile (RIP). The optical refractive indices of the inner core, inner-cladding and outer-core are the same and denoted by $n_{\rm core}$, $n_{\rm cladding}$ is the optical refractive index of the outer cladding layer. Correspondingly, the fibre shows a four-layer structure as acoustic waveguide with a w-shaped acoustic RIP. The acoustic refractive index N_i in the i-th doping layer is defined as[16]

$$N_i = V_{\rm l0}/V_{{\rm l}i}, \tag{1}$$

where $V_{\rm l0}$ and $V_{{\rm l}i}$ are the longitudinal acoustic velocities in pure silica cladding and the i-th layer, respectively.

The optical and acoustic RIP proposed in Fig. 1 can be realized by co-doping Al_2O_3 and GeO_2 in the inner core, inner cladding and outer core layers. Both Al_2O_3 and GeO_2 can increase the optical refractive index with respect to pure silica, but they have an opposite effect on acoustic properties: the former increases the acoustic velocity in silica and decreases the acoustic refractive index, while the latter decreases the acoustic velocity and increases the acoustic refractive index. By adjusting the concentrations of two dopants appropriately, the w-shaped acoustic RIP can be realized while the optical RIP maintains to be a simple step-like structure. The method of co-doping Al and Ge in optical fibre has been proven to be valid both in theory and in actual fabrication processes.[16] The changes of optical refractive index and longitudinal acoustic velocity for unit dopant concentration

are listed in Table 1,[17] by which the optical refractive index n and longitudinal acoustic velocity $V_{\rm l}$ in Al/Ge co-doped fibre can be calculated as

$$n = n_0(1 + 0.056 \times w_{\rm Ge} + 0.063 \times w_{\rm Al}), \quad (2)$$

$$V_{{\rm l}j} = V_{\rm l0}(1 - 0.47 \times w_{\rm Ge} + 0.42 \times w_{\rm Al}), \quad (3)$$

where $w_{\rm Ge}$ and $w_{\rm Al}$ are doping concentrations of GeO_2 and Al_2O_3, and $n_0 = 1.458$ and $V_{\rm l0} = 5944$ m/s are optical refractive index and longitudinal acoustic velocity in pure silica, respectively. Comparing with the relations given in Refs. [11] and [12], we find that equations (2) and (3) can utilize weight percent (wt%) as the unit of dopant concentration instead of molecular percent (mol%) for convenience of analysis.

Table 1. Influence of Al_2O_3 and GeO_2 doped in silica on optical refractive index and longitudinal acoustic velocity.

Dopant	$\Delta n\%/w\%$	$\Delta V_l\%/w\%$
GeO_2	+0.056	–0.47
Al_2O_3	+0.063	+0.42

3. Theoretical analysis method

3.1. Optical mode analysis

The optical field distribution in the w-shaped Al/Ge-co-doped fibre is similar to that of single mode fibre due to the same optical RIP and it is determined by the two-dimensional (2D) scalar-wave equation:

$$\nabla_t^2 E + (2\pi/\lambda)^2(n^2 - n_{\rm eff}^2)E = 0, \quad (4)$$

where $\nabla_t^2 = \partial^2/\partial x^2 + \partial^2/\partial y^2$ is the transverse Laplacian operator in the 2D triangular coordinate, λ is the optical wavelength in vacuum, n is the refractive index of the materials of the fibre depending on the different layers' dopants and $n_{\rm eff}$ is the effective refractive index of optical modes determined by the equation. The scalar-wave equation can be solved easily by the eigenvalue analysis in mathematical method, the eigenvalues ($n_{\rm eff}$) and the eigenfunctions (the spatial distribution of optical field $E(x, y)$) of the equation can be obtained at the meanwhile.

3.2. Acoustic mode analysis

The acoustic mode of the fibre can be obtained by solving the 2D scalar-wave equation about the displacement field $u(x, y)$:[12,16,18]

$$\nabla_t^2 u + (\omega_{\rm ac}^2/V_{\rm l}^2 - \beta_{\rm ac}^2)u = 0, \quad (5)$$

where $\omega_{\rm ac}$ and $V_{\rm l}$ are the angular frequency and the longitudinal acoustic velocity across the fibre, respectively, $\beta_{\rm ac}$ is the propagation constant of longitudinal acoustic modes, which is related to angular frequency $\omega_{\rm ac}^{(i)}$ and longitudinal velocity $V_{\rm l}^{(i)}$ of the i-th-order acoustic mode as $\omega_{\rm ac}^{(i)} = \beta_{\rm ac}V_{\rm l}^{(i)}$. The displacement field can be expressed as the combination of the first and second kind of Bessel functions ($J_0(x)$ and $N_0(x)$) or modified Bessel functions ($I_0(x)$ and $K_0(x)$) in different layers of the fibre, depending on the different solving regions of the longitudinal velocity of acoustic mode. The continuity and free boundary conditions of displacement fields and stress components are satisfied at the transition boundaries between any inner layers and the outer boundary of outer-cladding,[19,20] respectively, through which the eigenvalues of the wave equation can be obtained.

3.3. Brillouin gain spectrum calculation

The BGS in the optical fibre is a sum of the contributions of different acoustic modes. Each acoustic mode will backscatter the optical LP_{01} mode efficiently when the phase-matching condition, $\beta_{\rm ac} = 2\beta_{\rm op}$, is fulfilled, where $\beta_{\rm op}$ is the propagation constant of optical mode. The effective acousto-optic area, which is defined as the overlap integral between the optical LP_{01} mode and acoustic L_{0i} mode, is always used to evaluate the efficiency of the back-scattering process and is given by[21]

$$A_{\rm eff}^{{\rm ao}(i)} = [\langle E^2\rangle/\langle E^2u^{(i)}\rangle]^2\langle(u^{(i)})^2\rangle, \quad (6)$$

where E denotes the electric field and $u^{(i)}$ denotes the acoustic field. It is worth while to note that both the electric and acoustic field here is normalized by optical and acoustic power, respectively. The triangle brace $\langle f\rangle = \iint f\,{\rm d}x\,{\rm d}y$ denotes the integration of f over the whole cross-section plane of the optical fibre.

The i-th-order Brillouin gain coefficient $g^{(i)}$ related to the i-th-order acoustic mode is evaluated by the acousto-optic effect intensity $I^{(i)}$, which is defined as the reciprocal of $A_{\rm eff}^{{\rm ao}(i)}$:

$$g^{(i)} = 4\pi n_{\rm eff}^2/(p_{12}^2\lambda^3\rho c\nu_{\rm ac}^{(i)}\Delta\nu_{\rm ac}^{(i)}) \cdot I^{(i)}. \quad (7)$$

The i-th-order BGS is given by[18]

$$s_i(\nu) = g^{(i)} \cdot (\Delta\nu_{\rm ac}^{(i)}/2)^2/[(\nu - \nu_{\rm ac}^{(i)})^2 + (\Delta\nu_{\rm ac}^{(i)}/2)^2], \quad (8)$$

where p_{12} is the elastooptic constant, ρ is the density of material, c is the speed of light in vacuum, $\nu_{\rm ac}^{(i)}$ is the frequency of the i-th-order acoustic mode and $\Delta\nu_{\rm ac}^{(i)}$ is the full-width at half maximum (FWHM) bandwidth

of the i-th-order BGS that is contributed by the L_{0i} mode and is assumed to be the same as ∼35 MHz for all acoustic modes. It is clear that $s_i(\nu)$ has a Lorentzian profile. As the contributions of acoustic modes are statistically independent, the total BGS is expressed as

$$S(\nu) = \sum_i s_i(\nu), \tag{9}$$

with Eq. (9), the BGS of the optical fibre can be calculated numerically.

4. Acoustic mode coupling in Al/Ge-co-doped fibre

4.1. Dispersion relations and mode-coupling properties of longitudinal acoustic modes

A w-shaped Al/Ge-co-doped fibre design is presented in order to analyse the longitudinal mode coupling properties. The dopants concentrations in the core region are listed in Table 2. The inner core is only doped with GeO_2, while the inner-cladding and outer-core layers are both co-doped with GeO_2 and Al_2O_3, making the acoustic refractive indexes N_1, N_2, and N_3 being 1.072, 1.005, and 1.015 accordingly. It is noted that N_2 is a little greater than unity for the convenience of computation, which does not influence the analysis of physical prospect. The radii of these layers are $a_1 = 1$ μm, $a_2 = 2$ μm, and $a_3 = 4$ μm.

Table 2. The Al_2O_3 and GeO_2 concentrations in presented fibre.

Layers	GeO_2 concentration /wt%	Al_2O_3 concentration /wt%
Inner-core	14.3	0
Inner-cladding	8.50	8.32
Outer-core	9.66	7.29

The dispersion curves of $L_{01} \sim L_{07}$ acoustic modes are plotted in Fig. 2(a) as the acoustic refractive index N versus the normalized acoustic frequency $V_{\rm ac}$, which is defined as

$$V_{\rm ac} = \beta_{\rm ac} a_1 V_{l4} \sqrt{(1/V_{l1})^2 - (1/V_{l4})^2}. \tag{10}$$

It is clear that there are several acoustic longitudinal mode-coupling regions along the $V_{\rm ac}$ axis, and two or more mode-coupling points may exist around one $V_{\rm ac}$ value, corresponding to the same $\beta_{\rm ac}$. The value of $V_{\rm ac}$ around the L_{02} and L_{03} mode coupling point corresponds to the case under a pump wavelength of 1.55 μm, and the corresponding BGS is shown in Fig. 2(b). The coupling L_{02} and L_{03} acoustic modes make remarkable contributions to the Brillouin gain and the dual-peak structure of BGS is obvious at the frequency domain between 11.8 GHz and 12.0 GHz.

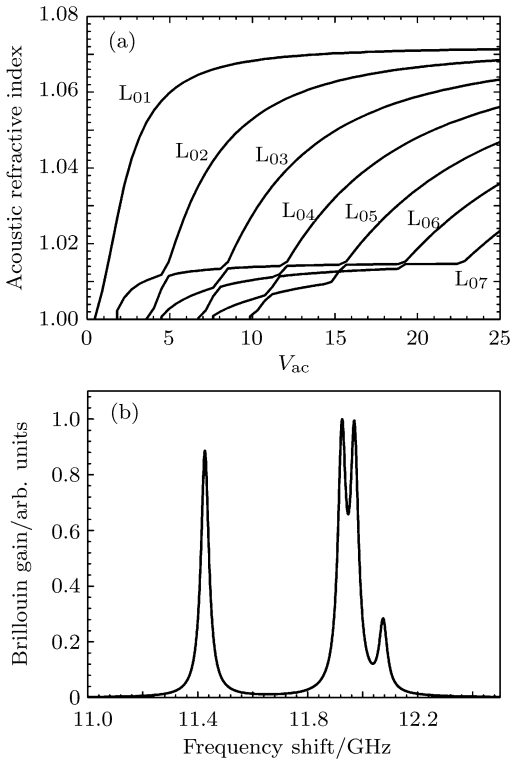


Fig. 2. (a) Acoustic dispersion curves of acoustic refractive index N as functions of $V_{\rm ac}$. (b) The BGS under the pump wavelength of 1.55 μm, corresponding to the L_{02} and L_{03} mode coupling point.

In order to illustrate the longitudinal mode coupling clearly, the acoustic waveguide structure of the fibre is decomposed into two simpler ones, one only has inner core and the other only has outer core. The solid and dashed lines in Fig. 3(a) denote the acoustic RIPs of the two assumed acoustic waveguides. The corresponding dispersion curves of longitudinal acoustic modes of these two waveguides are shown in Fig. 3(b). The cross points of two clusters of curves with respect to the two waveguide structures agree well with the mode-coupling points in Fig. 2(a), which indicate that the longitudinal acoustic mode coupling in the w-shaped Al/Ge-co-doped fibre is induced by the coupling between the acoustic longitudinal modes supported by the inner-core and outer-core waveguide structures.

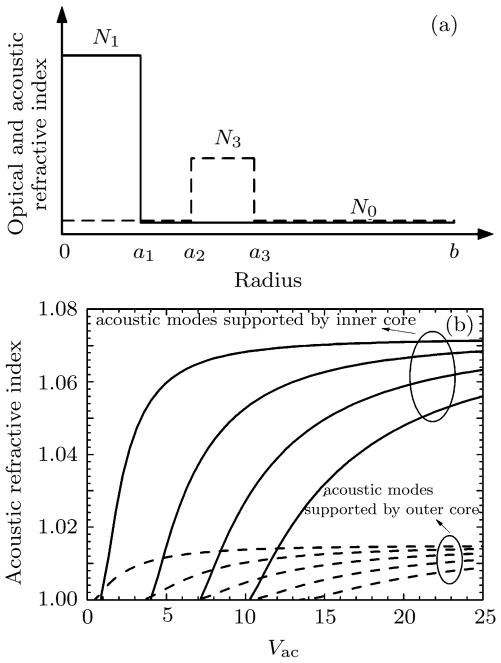


Fig. 3. Two assumed structures of acoustic waveguides composing of the w-shaped Al/Ge-co-doped fibre: (a) acoustic RIPs of two waveguides; (b) modal dispersion curves of two acoustic waveguides.

4.2. Influences of structural and material parameters on longitudinal acoustic mode coupling properties

The acoustic mode coupling properties of the proposed w-shaped Ge/Al-co-doped fibre structure can be designed by modifying the doping concentrations of each layer to realize a proper acoustic RIP, which can be fabricated by using conventional fibre technology.

Figure 4 shows the acoustic dispersion curves with different radii and doping concentrations of outer-core layer. All the structural and material parameters are the same with those in Fig. 2(a) except for $a_3 = 6$ μm in Fig. 4(a) and $N_3 = 1.05$ in Fig. 4(b), respectively. Here we define the thickness of inner core, inner-cladding, outer-cladding as $d_1 = a_1$, $d_2 = a_2 - a_1$, $d_3 = a_3 - a_2$, respectively, for the convenience of discussion. It can be seen that as d_3 increases, the dispersion curves corresponding to the acoustic modes supported by the outer core layer move toward the left side of V_{ac} axis and the curves become denser. This is because increasing d_3 means the increasing size of acoustic waveguide of the outer core, leading to an effective acoustic refractive index enhancement of each mode and an amount of increase of acoustic modes supported by it. On the other hand, the increase of doping concentration in the outer core layer makes all the effective acoustic indices of acoustic modes supported by the outer core higher, just as shown in Fig. 4(b), in addition, the cut-off condition of these acoustic modes is also changed. It can be expected that similar changes of structural and material parameters for the inner-core layer will lead to similar variations on acoustic modes supported by inner-core layer. As a result, the positions of acoustic mode coupling points can be adjusted flexibly by modifying the sizes and doping concentrations of inner-core and outer-core layers.

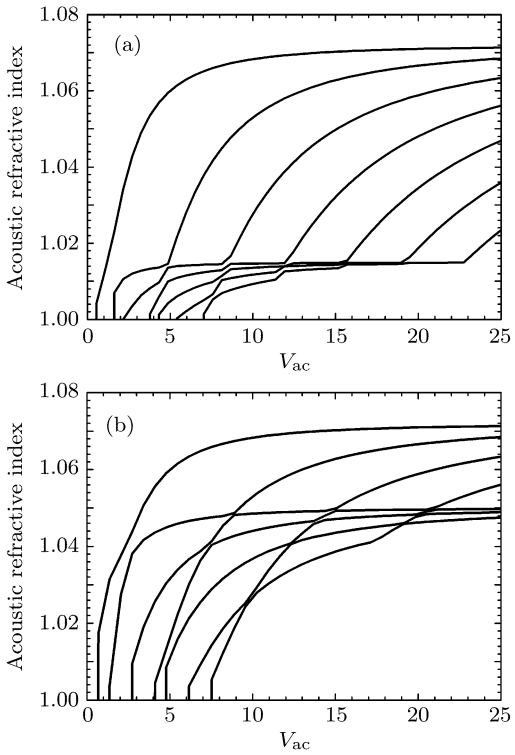


Fig. 4. Acoustic dispersion curves at (a) $d_3 = 4$ μm and (b) $N_3 = 1.05$, with all other parameters invariable comparing with those in Fig. 2(a).

Figure 5(a) is the comparison of acoustic dispersion curves when d_2 is 1 μm and 0.3 μm, with d_1, d_3, and N_i being the same as those in Fig. 2(a). The dispersion curves are similar to each other except for the coupling point between the L_{02} and L_{03} modes. It can be seen that the mode coupling intensity becomes stronger when d_2 is reduced, as the detail around the mode coupling point shown in Fig. 5(b). It can be explained by the coupling intensity enhancement between the acoustic modes supported by the inner-core and outer-core layers, respectively, when the two acoustic waveguides are closer as d_2 decreases. Hence, adjusting the thickness of inner-cladding layer is an effective way to adjust the intensity of acoustic mode coupling in the fibre.

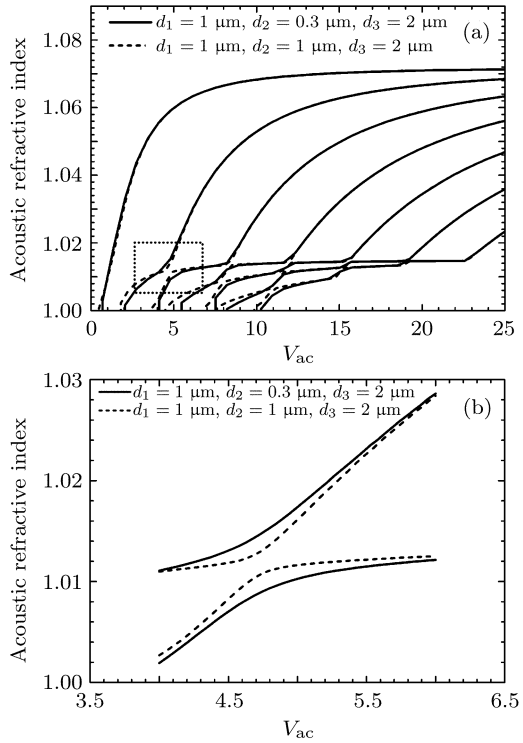


Fig. 5. Influences of structural parameters d_2 on the acoustic mode coupling properties: (a) acoustic dispersion curves with $d_2 = 0.3$ μm and $d_2 = 1$ μm, while d_1, d_3, and N_i being the same with those in Fig. 2(a); (b) details of dispersion curves around L_{02} and L_{03} acoustic mode coupling point, showing an obvious change of mode coupling intensity under different d_2.

5. Fibre design for distributed temperature and strain sensing

The relations between acoustic dispersion curves and structural and material parameters of the fibre indicate that it is possible to design the position of acoustic mode coupling point and coupling intensity to realize special multi-peak BGS, which has potential application in distributed fibre Brillouin sensing of multi-physical variables.

A w-shaped Al/Ge-co-doped optical fibre design aiming at distributed sensing at 1.55 μm is proposed here. The structural parameters for this fibre are $a_1 = 1$ μm, $a_2 = 2.2$ μm, $a_3 = 5$ μm, while the effective acoustic refractive indices are $N_1 = 1.0648$, $N_2 = 1.002$, and $N_3 = 1.05$ respectively. The corresponding dopants concentrations in each layer of fibre are listed in Table 3.

Figure 6(a) is the acoustic dispersion curves in the fibre, in which the dashed line corresponds to the pump wavelength of 1.55 μm. It can be seen that the lowest acoustic modes of inner and outer core (L_{01} and L_{02} acoustic modes) are coupling, generating two lowest peaks in the BGS at 1.55 μm, which is shown in Fig. 6(b). The parameter optimization of the design considers that the frequency difference of two main gain peaks should be far enough to ensure that they can be discriminated, while, the two gain peaks should have a proper intensity difference, which is about 3 dB shown in Fig. 6(b), to enhance its sensitivity to environmental variations.

Table 3. Al_2O_3 and GeO_2 concentrations in the fibre for temperature and strain sensing.

Layers	GeO_2 concentration /wt%	Al_2O_3 concentration /wt%
Inner-core	12.95	0
Inner-cladding	6.56	6.87
Outer-core	11.97	2.06

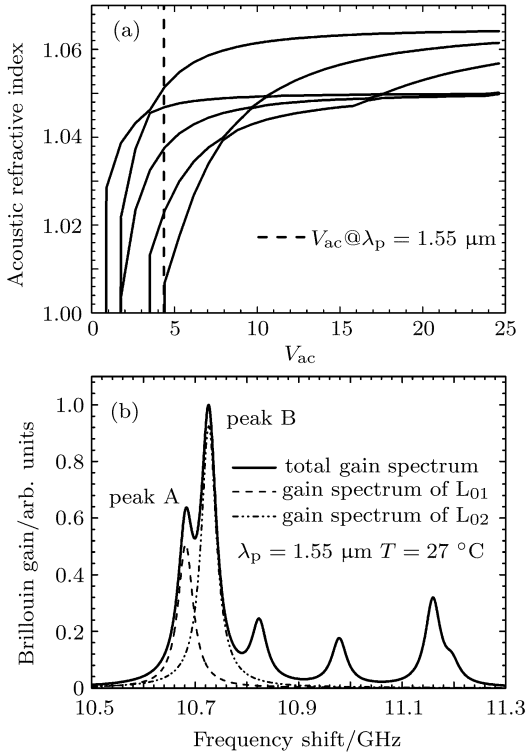


Fig. 6. (a) Acoustic dispersion curves of L_{01}–L_{05} modes of fibre with pump wavelength being away from the acoustic mode coupling point. The dash line marks the value of V_{ac} corresponding to the pump wavelength of 1.55 μm. (b) The BGS with two main peaks having an intensity difference.

To demonstrate the potential of the fibre design for distributed fibre Brillouin sensing of multi-physical variables, we calculate the BGSs of the proposed fibre structure under different temperature and tensile strains, showing the changes of the intensity ratio and

Brillouin frequency shifts (BFS) of the two gain peaks in the BGS with environmental variation.

The relationship of material properties of fused silica, including the refractive index n, material density ρ, Young's modulus E, and Poisson ratio γ, as the temperature change are given as[22]

$$n = 1.45742 + 2.1233 \times 10^{-5}t + 0.6 \times 10^{-8}t^2, \quad (11)$$

$$\rho = 2201.8913 - 4.0358 \times 10^{-3}t + 3.86 \times 10^{-7}t^2, \quad (12)$$

$$E = (7.20587 + 1.285 \times 10^{-3}t - 4.4978 \times 10^{-7}t^2) \times 10^{10}, \quad (13)$$

$$\gamma = 0.16894 + 2.8162 \times 10^{-5}t - 2.0696 \times 10^{-9}t^2, \quad (14)$$

where t denotes temperature in unit of °C. The changes of material parameters in turn influence the Brillouin gain properties. The BFS and intensity ratio of two gain peaks under the pump wavelengths of 1.55 μm are shown in Fig. 7. The values of gain peaks for calculating the intensity ratio are obtained by making Lorentz fitting of each peak. Figure 7(a) shows that the peak intensity ratio decreases with increasing temperature by a coefficient of –0.02328 dB/°C, and Brillouin frequency shifts rise with slopes of 1.24 MHz/°C both for peaks A and B, respectively, as shown in Fig. 7(b).

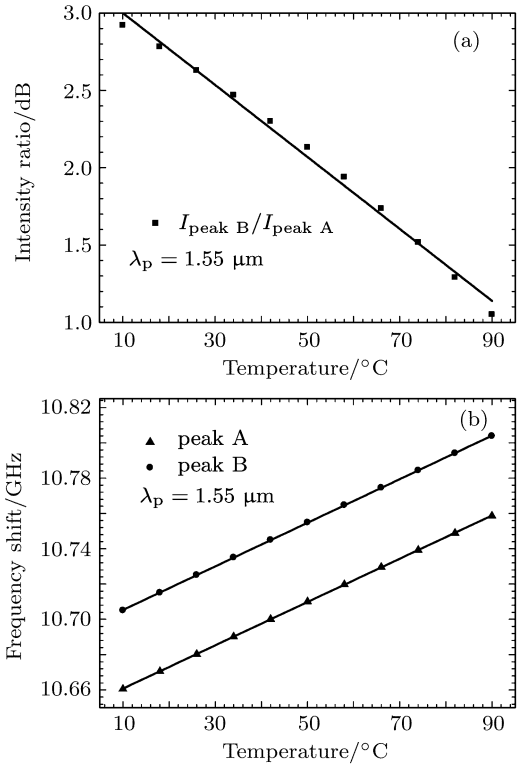


Fig. 7. (a) Intensity ratio and (b) Brillouin frequency shifts of two main gain peaks versus the environmental temperature under a pump wavelength of 1.55 μm.

The strain applied on the fibre can also influence the Brillouin properties remarkably. Different kinds of strain will affect the acoustic fields in the fibre in different ways. Here, we take the tensile strain as an example for analysing its influence on the mode coupling properties. The tensile strain is induced by the elongation of a piece of length of fibre and the induced strain is expressed as the fibre length change divided by the initial length $\Delta L/L_0$. The parameters of materials of fibre will change when the strain is applied:[23–25]

$$n = n_0\{1 - (n_0^2/2) \cdot [p_{12} - \gamma(p_{11} + p_{12})]\varepsilon\}, \quad (15)$$

$$\rho = \rho_0/[(1+\varepsilon)(1-\gamma\varepsilon)^2], \quad (16)$$

$$E = E_0(1 + \alpha\varepsilon), \quad (17)$$

$$\gamma = \gamma_0(1 + k\varepsilon), \quad (18)$$

where n_0, ρ_0, E_0, γ_0 are values of the corresponding parameters of pure silica free of strain and at room temperature, respectively, ε is the induced tensile strain in arbitrary unit, p_{11} and p_{12} are lateral and longitudinal elastooptic coefficients, respectively, α (=8.7) and k (=22) are strain coefficient of Young's modulus and Poisson strain coefficient, respectively. The changes of BFS and intensity ratio of two gain peaks as the increasing strain under the pump wavelengths of 1.55 μm are shown in Fig. 8. The intensity ratio of two gain peaks increases with increasing tensile strain by a coefficient of 2.060×10^{-4} dB/με, while the Brillouin frequency shifts of both peaks A and B increase by a coefficient of 0.0688 MHz/$\mu\varepsilon$.

It is seen that the Brillouin gain peak intensity ratio and BFS in the w-shaped Al/Ge-co-doped fibre have two independent responses to environmental temperature and applied tensile strain, which can be used to realize the distributed temperature and strain sensing through measuring the intensity ratio and Brillouin frequency shifts of the fibre. The variation of peak intensity ratio ΔR_{peak} and BFS $\Delta\nu_{\text{B}}$ can be written as the functions of the change of temperature ΔT and that of strain $\Delta\varepsilon$:

$$\Delta R_{\text{peak}} = C_R^T \Delta T + C_R^\varepsilon \Delta\varepsilon, \quad (19)$$

$$\Delta\nu_{\text{B}} = C_\nu^T \Delta T + C_\nu^\varepsilon \Delta\varepsilon, \quad (20)$$

where C_R^T and C_R^ε are the temperature and strain coefficient of peak intensity ratio, C_ν^T and C_ν^ε are the temperature and strain coefficient of BFS, respectively, and their values are given in the above discussion.

Thus the measurment parameters ΔT and $\Delta\varepsilon$ for sensing can be expressed in the form of matrix equations as

$$\begin{bmatrix} \Delta T \\ \Delta\varepsilon \end{bmatrix} = \frac{1}{|A|} \begin{bmatrix} C_\nu^\varepsilon & -C_R^\varepsilon \\ -C_\nu^T & C_R^T \end{bmatrix} \begin{bmatrix} \Delta R_{\text{peak}} \\ \Delta\nu_{\text{B}} \end{bmatrix}, \quad (21)$$

where $|A| = C_R^T C_\nu^\varepsilon - C_\nu^T C_R^\varepsilon$. The value of $|A|$ is nonzero because of the opposite signs of C_R^T and C_R^ε. Considering the typical measurement errors in Brillouin sensing as $\Delta R_{\text{peak}} = 1\%$ (about 0.04 dB) and $\Delta\nu_{\text{B}} = 0.5$ MHz, we find that the errors of discriminative measurement of temperature and strain are about 1.4 °C and 33 $\mu\varepsilon$, respectively.

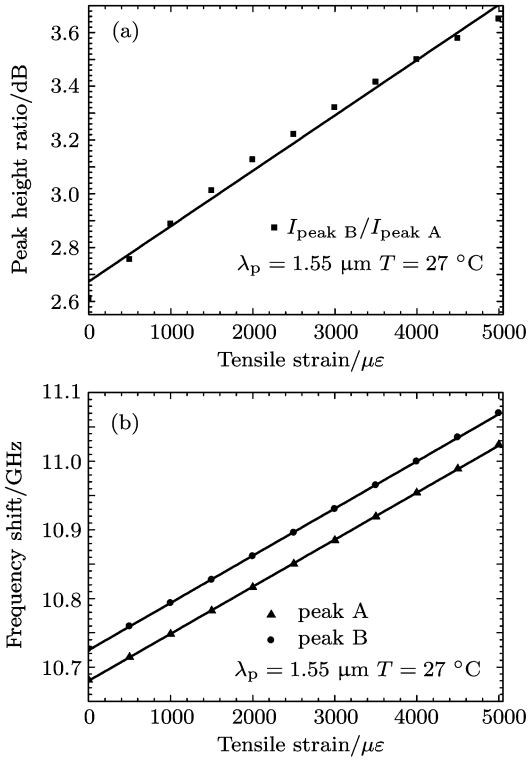


Fig. 8. (a) Intensity ratio and (b) Brillouin frequency shifts of two main gain peaks versus the tensile strain applied on the fibre under a pump wavelength of 1.55 μm.

Comparing several other kinds of fibres, we find that the calculated temperature and strain sensing errors of the proposed Al/Ge-co-doped fibre have the same magnitude as those of MSF, PMF and w-shaped triple-layer fibre,[12,26–28] and are much better than that of large effective area fibre.[29] The MSF and PMF are not suitable for the application of long-distance distributed fibre sensing because of their high cost due to the complicated manufacturing process. However, in the the w-shaped triple-layer fibre experiment the 4th gain peak of BGS was used, whose intensity is much lower than the main peak by 20 dB,[12,28] leading to the difficulty in weak sensing signal detection.

The proposed fibre utilizes the 1st and 2nd Brillouin gain peaks for sensing, which are formed by the coupling of fundamental acoustic modes in inner-core and outer-core regions, namely the L_{01} and L_{02} acoustic modes, respectively. The intensities of the two gain peaks are close, and it is easy to detect the sensing signal and achieve small sensing errors. The proposed fibre can be conveniently fabricated through traditional silica fibre manufacturing processes, which has favourable potential in the application of long-distance distributed temperature and strain sensing because of its low cost.

6. Conclusion

A novel fibre structure aiming at distributed temperature and strain sensing is proposed in this paper. Utilizing Al_2O_3 and GeO_2 as dopants to form a w-shaped acoustic waveguide, we realized the modal coupling between longitudinal acoustic modes of its inner and outer core layers, leading to dual-peak or multi-peak BGS. A specific fibre design realizing the multi-peak BGS is given, showing the two main gain peaks with an intensity difference under a pump wavelength of 1.55 μm. The responses of BGS properties on temperature and strain are analysed theoretically, showing its potential in the distributed fibre Brillouin sensing for temperature and strain simultaneously.

References

[1] G P Agrawal 2007 *Nonlinear Fibre Optics* 4th edn. (Boston: Elsevier/Academic Press) pp. 222–243

[2] Geng D, Yang D X, Shen G F and Zhang X M 2008 *Chin. Phys.* B **17** 1020

[3] Zhang Z X, Wu J, Xu K, Hong X B and Lin J T 2010 *Chin. Phys.* B **19** 064209

[4] Ohashi M, Shibata N and Shiraki K 1992 *Electron. Lett.* **28** 900

[5] Okawachi Y, Bigelow M S, Sharping J E, Zhu Z M, Schweinsberg A, Gauthier D J, Boyd R W and Gaeta A L 2005 *Phys. Rev. Lett.* **94** 153902

[6] Horiguchi T, Kurashima T and Tateda M 1990 *IEEE Photon. Technol. Lett.* **2** 352

[7] Kurashima T, Horiguchi T and Tateda M 1990 *Opt. Lett.* **15** 1038

[8] Nikles M, Thevenaz L and Robert P A 1996 *Opt. Lett.* **21** 758

[9] Bao X, DeMerchant M, Brown A and Bremner T 2001 *J. Lightw. Technol.* **19** 1698

[10] Soto M A, Bolognini G and Pasquale F D 2009 *IEEE Photon. Technol. Lett.* **21** 450

[11] Koyamada Y, Sato S, Nakamura S, Sotobayashi H and Chujo W 2004 *J. Lightw. Technol.* **22** 631

[12] Zou W, He Z, Kishi M and Hotate K 2008 *Opt. Express* **16** 10006

[13] Zou W, He Z and Hotate K 2009 *Opt. Express* **17** 1248

[14] Dainese P, Russell P S J, Joly N, Knight J C, Wiederhecker G S, Fragnito H L, Laude V and Khelif A 2006 *Nat. Phys.* **2** 388

[15] Zhang W, Wang Y, Pi Y, Huang Y and Peng J 2007 *Opt. Lett.* **32** 2303

[16] Li M, Chen X, Wang J, Gray S, Liu A, Demeritt J A, Ruffin A B, Crowley A M, Walton D T and Zenteno L A 2007 *Opt. Express* **15** 8290

[17] Jen C K, Neron C, Shang A, Abe K, Bonnell L and Kushibiki J 1993 *J. Am. Ceram. Soc.* **76** 712

[18] Tartara L, Codemard C, Maran J, Chief R and Zghal M 2009 *Opt. Commun.* **282** 2431

[19] Auld B A 1990 *Acoustic Fields and Waves in Solids* 2nd edn. Vol. I (FL: Krieger) p. 498

[20] Waldron R A 1969 *IEEE Trans. Microwave Theory Tech.* **MIT-17** 893

[21] Kobyakov A, Kumar S, Chowdhury D Q, Ruffin A B, Sauer M and Bickham S R 2005 *Opt. Express* **13** 5338

[22] Zhao L J, Li Y Q, Li Z M, He Y J, Zhang F C and Yoshino T 2006 *Proc. 1st IEEE Int. Conf. Nano/Micro Engineering and Molecular Systems* (NEMS) January 18–21, 2006, Zhuhai, China p. 1327

[23] Zhang C, Li W and Bao X 2007 *Opt. Lett.* **32** 2565

[24] Horiguchi T, Kurashima T and Tateda M 1989 *IEEE Photon. Technol. Lett.* **1** 107

[25] Bertholds A and Dandliker R 1987 *J. Lightw. Technol.* **LT-5** 895

[26] Zou L, Bao X, Afshar V S and Chen L 2004 *Opt. Lett.* **29** 1485

[27] Zou W, He Z and Hotate K 2010 *IEEE Photon. Technol. Lett.* **22** 526

[28] Zou W, He Z, Kishi M and Hotate K 2007 *Opt. Lett.* **32** 600

[29] Alahbabi M, Cho Y T and Newson T P 2004 *Opt. Lett.* **29** 26